12. E. R. Mueller, R. Henschke, W. E. Robotham, Jr., L. A. Newman, L. M. Laughman, R. A. Hart, J. Kennedy, and H. M. Pickett, "Terahertz local oscillator for the Microwave Limb Sounder on the Aura satellite," Appl. Opt. **46**(22), 4907–4915 (2007).
13. U. U. Graf, S. Heyminck, R. Güsten, P. Hartogh, H.-W. Hübers, K. Jacobs, M. Philipp, D. Rabanus, H.-P. Röser, J. Stutzki, P. Van der Wal, and A. Wagner-Gentner, "GREAT: the German first light heterodyne instrument for SOFIA," in Proc. Conf. on Millimeter and Submillimeter Detectors for Astronomy III, vol. SPIE 6275, Orlando, 2006, pp. 62750K–1-62750K–7.
14. M. Wienold, L. Schrottke, M. Giehler, R. Hey, W. Anders, and H. T. Grahn, "Low-voltage terahertz quantum-cascade lasers based on LO-phonon-assisted interminiband transitions," Electron. Lett. **45**(20), 1030–1031 (2009).
15. L. Schrottke, M. Giehler, M. Wienold, R. Hey, and H. T. Grahn, "Compact model for the efficient simulation of the optical gain and transport properties in THz quantum-cascade lasers," Semicond. Sci. Technol. **25**(4), 045025 (2010).
16. A. M. Veprik, S. V. Riabzev, G. S. Vilenchik, and N. Pundak, "Ultra-low vibration split Stirling linear cryogenic cooler with a dynamically counterbalanced pneumatically driven expander," Cryogenics **45**(2), 117–122 (2005).
17. L. L. Bonilla, and H. T. Grahn, "Nonlinear dynamics of semiconductor superlattices," Rep. Prog. Phys. **68**(3), 577–683 (2005).
18. E. Bründermann, M. Havenith, G. Scalari, M. Giovannini, J. Faist, J. Kunsch, L. Mechold, and M. Abraham, "Turn-key compact high temperature terahertz quantum cascade lasers: imaging and room temperature detection," Opt. Express **14**(5), 1829–1841 (2006).
19. D. Rabanus, U. U. Graf, M. Philipp, O. Ricken, J. Stutzki, B. Vowinkel, M. C. Wiedner, C. Walther, M. Fischer, and J. Faist, "Phase locking of a 1.5 Terahertz quantum cascade laser and use as a local oscillator in a heterodyne HEB receiver," Opt. Express **17**(3), 1159–1168 (2009).
20. P. Khosropanah, A. Baryshev, W. Zhang, W. Jellema, J. N. Hovenier, J. R. Gao, T. M. Klapwijk, D. G. Paveliev, B. S. Williams, Q. Hu, J. L. Reno, B. Klein, and J. L. Hesler, "Phase locking of a 2.7 THz quantum cascade laser to a microwave reference," Opt. Lett. **19**(34), 2958–2960 (2009).
21. H. Richter, S. G. Pavlov, A. D. Semenov, L. Mahler, A. Tredicucci, H. E. Beere, D. A. Ritchie, and H.-W. Hübers, "Sub-megahertz frequency stabilization of a terahertz quantum cascade laser to a molecular absorption line," Appl. Phys. Lett. **96**(7), 071112 (2010).

## 1. Introduction

Terahertz (THz) quantum-cascade lasers (QCLs) are very promising radiation sources for many scientific and commercial applications. Examples are high-resolution spectroscopy in atmospheric research or astronomy and imaging in the fields of security, non-destructive testing, and biomedicine. Since the first demonstration of a THz QCL in 2002 [1], its performance has been rapidly improved with respect to output power, operating temperature, and frequency coverage [2]. Recently, the applicability of QCLs for imaging either in close-by configuration [3–5] or at stand-off distances [6] as well as the feasibility of high-resolution molecular spectroscopy [7] has been principally demonstrated. For these applications, the QCLs are either operated in a continuous-flow liquid-helium cryostat or in a liquid-helium-free mechanical cryocooler [8], which has, however, several disadvantages. On the one hand, the cooling capacity of a liquid-helium flow cryostat is rather limited, which prevents continuous-wave (cw) operation of QCLs with rather large pumping power. In addition, cooling with liquid helium is expensive and requires experience and safety measures. In fact in the imaging experiment described in [4], the operational duty cycle of the laser was 1%. On the other hand, QCLs in mechanical cryocoolers can be operated in cw mode. However, cryocoolers are bulky and require several kW electrical power in order to provide sufficient cooling capacity for the QCL, which typically uses an electrical pump power of several Watts for a THz emission power of several mW. While these cooling approaches might be acceptable for scientific experiments in the laboratory, they are impractical for most commercial applications.

The implementation of QCLs as local oscillators (LOs) in heterodyne spectrometers for remote sensing with high spectral resolution [9, 10] is another potential application. THz heterodyne spectroscopy is a powerful technique. Many space- or airborne missions are equipped with THz heterodyne spectrometers [11]. For example, the Aura satellite uses a heterodyne spectrometer to monitor stratospheric OH at a frequency of 2.5 THz. The LO is an optically pumped gas laser [12]. Similarly, the LO for the heterodyne receiver GREAT (German Receiver for Astronomy at Terahertz Frequencies) on board of SOFIA (Stratospheric Observatory for Infrared Astronomy) is a gas laser for frequencies above 3

THz [13]. Although these LOs are sophisticated devices, they are relatively large and lack frequency tunability.

For all of the aforementioned applications, QCLs have several advantages over other sources. In particular, they are frequency tunable, small, and require low electrical input power. However, liquid-helium cooling or cooling with bulky cryocoolers requiring large electrical power are impractical for air- and spaceborne or commercial applications. In this article, we report on the development of a compact, easy-to-use, cw THz source, which is based on a QCL operating at 3.1 THz and a compact, low-input-power Stirling cooler with a nominal cooling capacity of 7 W at 65 K. The QCL has been designed to comply with these thermal requirements. The performance of the system and initial results of imaging and spectroscopy experiments are presented.

## 2. Experimental setup

The QCL was developed for cw operation with an output power of several mW at temperatures above 50 K. At the same time, the pumping power is kept sufficiently low for integration into the Stirling cooler. The active region is based on a two-miniband design, in which efficient injection into the upper laser level is achieved by an intersubband transition resonant to the energy of the longitudinal optical phonon. The operating electrical field strength lies between 5 and 6 kV/cm, which is about half the value for the conventional designs that are based on scattering of electrons on longitudinal optical phonons. The low operating voltage and the low current density (about several hundred $A/cm^2$) guarantee pumping powers below 7 W for the employed laser with a 100-µm-wide, 11-µm-thick, and 1.43-mm-long ridge.

The active region of the QCL consists of 85 periods with each period containing nine GaAs quantum wells and nine $Al_{0.15}Ga_{0.85}As$ barriers [14] and is sandwiched between a 700-nm-thick, Si-doped ($2\times10^{18}$ $cm^{-3}$) GaAs bottom contact layer and a 80-nm-thick, highly Si-doped ($5\times10^{18}$ $cm^{-3}$) top contact layer. The complete structure was grown by molecular-beam epitaxy on a semi-insulating GaAs(100) substrate. The two Si-doped layers form a single-plasmon (SP) waveguide. The electrical contacts are wire-bonded to the top layer and to both sides of the laser ridge. The chip with the QCL was soldered with indium on a gold-plated copper submount. The laser has a Fabry-Pérot cavity with both facets uncoated. A more detailed description of the QCL is given in [14]. The current for the QCL was supplied by a home-made, battery-driven current source.

Using a compact model based on the self-consistent solution of the Schrödinger and Poisson equations in the framework of a one-dimensional scattering-rate approach for the simulation of gain and transport properties [15], the design was optimized in such a way that a sufficiently large calculated gain was obtained with values above 50 $cm^{-1}$ over a rather wide range of field strengths around 5 kV/cm.

The QCL is integrated into a commercial miniature cryocooler (model K535 from Ricor) [16]. This is a twin-piston, linear-integrated Stirling cooler operating with a 45 Hz cycle, which is dynamically balanced in order to minimize mechanical vibrations. Their amplitude in the displacer's direction is below 100 µm (corresponding to 0.1 N [16]), which is much less than the Rayleigh range of approximately 10 mm of the optical system described in section 4. The cooler has a nominal cooling capacity of 7 W at 65 K for an ambient temperature of 23°C. It weighs 9.5 kg and has the dimensions 32.1×13.9×27.4 $cm^3$ (length × width × height). The power supply for the cooler unit weighs 2.6 kg and has the dimensions 10.2×13.0×33.6 $cm^3$. The average electrical input power measured over five hours continuous operation was 220 W. It is cooled with tap water at a flow rate between 1 and 4 l/min.

The submount with the QCL is attached to a second copper mount, which in turn is fixed to the cold finger of the Stirling cooler. In order to ensure tight thermal contacts, indium foil is placed between the two copper mounts as well as between the second copper mount and the cold finger. The temperature is measured with a Si diode thermometer installed close to the QCL submount. Variations induced by the 45 Hz operation cycle are less than 0.1 K. As expected, the Fourier spectrum of the temperature variations exhibits a peak at 45 Hz. Higher

harmonics were not observed. Cold finger, copper mounts, and the QCL are encapsulated in a vacuum housing. Prior to operation, the housing is evacuated to a pressure of less than 1 Pa. The output window is made from z-cut quartz. In order to avoid standing waves and to minimize Fabry-Pérot type etalon effects in the setup and back reflections into the laser, the output window is somewhat tilted with respect to the optical axis. When the QCL is turned off, the cooler reaches its minimum temperature of 24 K approximately 25 min after it is switched on.

## 3. System performance

Figure 1 shows the current-voltage and the light-current characteristics with a starting temperature of 54 K and an end temperature of 58 K. The emission from the QCL is measured with a Golay cell detector. When the laser turns on, the lowest operating temperature that can be achieved with the Stirling cooler is approximately 35 K. At this temperature, the lasing threshold occurs at 300 mA and 6 V. This corresponds to an electrical input power of 1.8 W and a threshold current density of 210 A/cm$^2$. The output power is maximal in the range from 600 to 650 mA (approximately 5.0 to 5.8 W electrical input power), and the laser intensity decreases above 650 mA. The maximal output power is 8 mW measured with a Thomas Keating opto-acoustic power meter in front of the vacuum window of the cooler. The steps in the output power are probably caused by electric-field domains, which can occur in doped or photoexcited semiconductor superlattices [17].
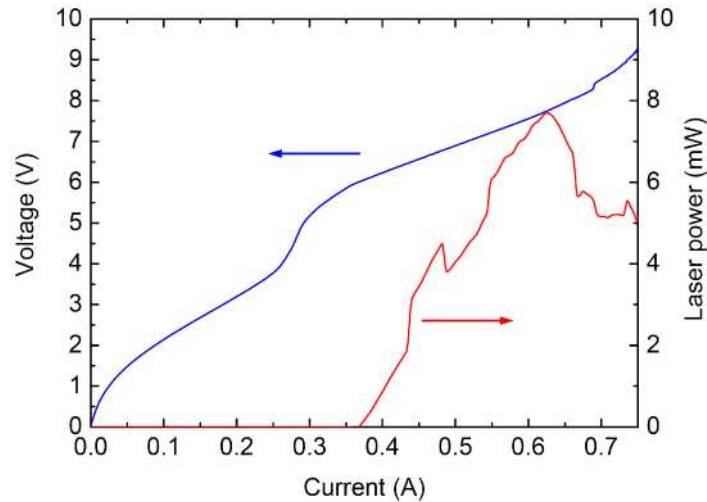


Fig. 1. Voltage and output power of the QCL as a function of current with a starting temperature of 54 K and an end temperature of 58 K. The steps in the output power are probably caused by electric-field domains.
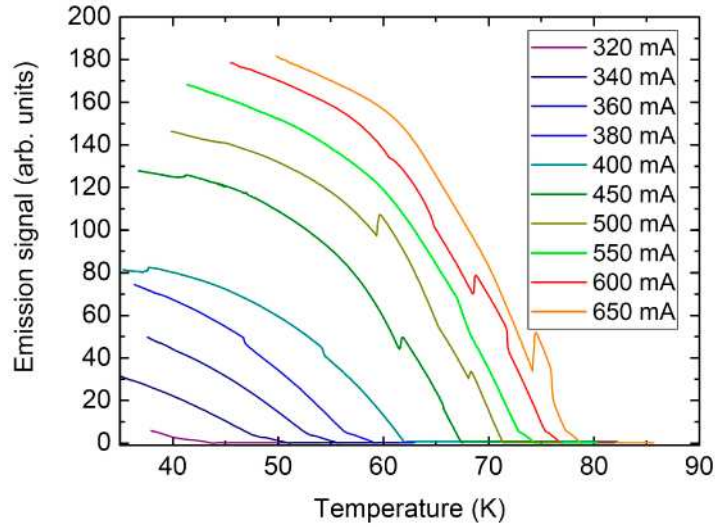
Fig. 2. Cw laser output signal as a function of temperature for several driving currents.

The output power is shown in Fig. 2 as a function of temperature for several driving currents. The laser signal was measured with a liquid-helium-cooled Ge:Ga photoconductive detector. The laser was first cooled to the lowest operating temperature. Then the Stirling cooler was switched off, and the output power was measured as a function of temperature. A clear increase of the output power and maximum operating temperature is observed for increasing current values up to 650 mA. In this regime, the increase of the laser gain apparently overcompensates the thermally induced losses inside the laser.
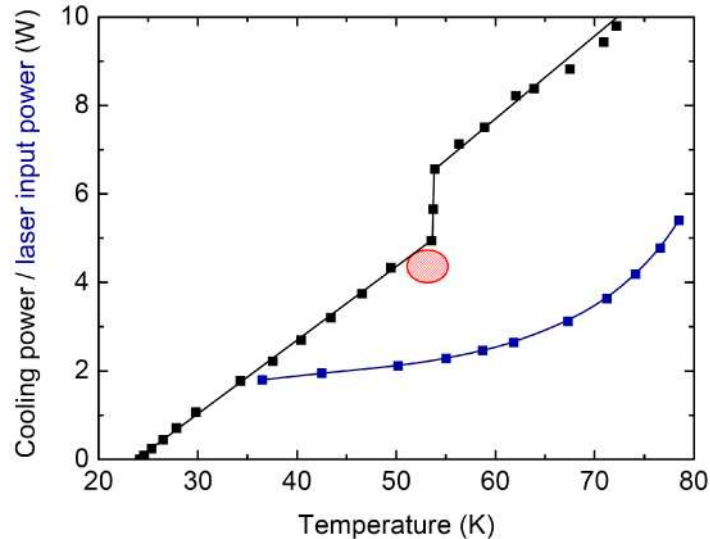


Fig. 3. Electrical input power at lasing threshold of the QCL (blue curve) and cooling power available from the Stirling cooler (black curve) as a function of temperature. The step at 54 K occurs because the internal temperature stabilization of the cooler does not function below this temperature. Across the whole range, the electrical input power at the temperature threshold is much less than the available cooling power. The red ellipse indicates the region of maximum output power.

In Fig. 3, the electrical input power at lasing threshold is plotted as a function of temperature along with the cooling power available from the Stirling cooler. The cooling

power was measured by resistive heating of the cold finger. The step at 54 K appears because the internal temperature stabilization of the cooler does not function below this temperature so that a stable operation mode with less cooling power prevents damage to the cooler. Across the whole temperature range, the electrical input power at laser threshold is much less than the available cooling power. At 78.6 K laser operation stops. However, the cooling power at this temperature is still above the electrical input power indicating that the laser operation terminates for intrinsic reasons rather than due to a limited cooling capacity. Note that the highest operating temperature is slightly above the boiling point of liquid nitrogen (77.4 K) so that operation with approximately 200 µW output power is expected at this temperature. As an example for the effectiveness of the Stirling cooler, a constant temperature of 52 K is reached after 15 min of laser operation for a current value of 650 mA.
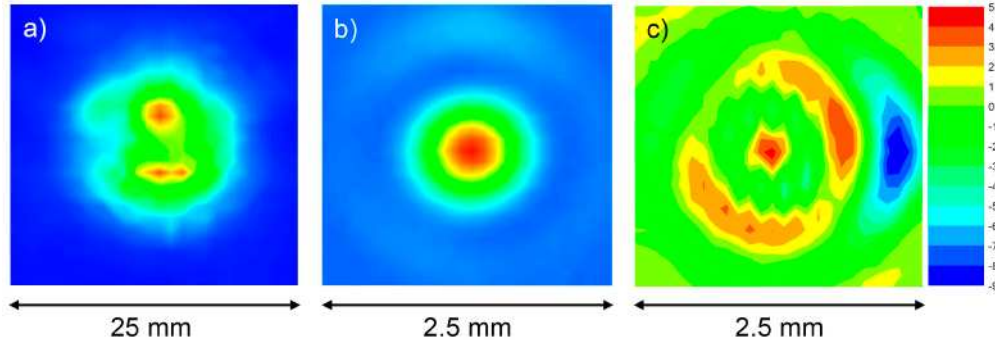


Fig. 4. Beam profiles of the QCL. (a) Beam profile measured at 2.5 cm distance from the QCL. Two emission maxima (red) can be distinguished. One originates directly from the laser ridge, and the other one comes from the substrate. (b) Beam profile at the position of the minimum waist created by a lens in front of the QCL. (c) Residual of the measured beam profile from (b) and a fitted Gaussian profile normalized to the peak intensity. The deviation is between + 4.5% and −8.8% (cf. legend on the right side).

The beam profile of the QCL was measured by scanning a Golay cell detector with an aperture of 1 mm diameter in a plane orthogonal to the emission direction of the QCL at 2.5 cm distance. As shown in Fig. 4(a), two emission lobes can be distinguished. The upper one is almost circular, while the lower one has an elongated, slightly curved shape. As has been shown in previous publications, these lobes can be attributed to emission from the substrate, into which part of the laser mode extends, and from the active medium itself [10, 18]. The surrounding of the back facet and parts of the copper submount were covered with non-transmitting material, in order to minimize residual reflections, which may cause interference structures.
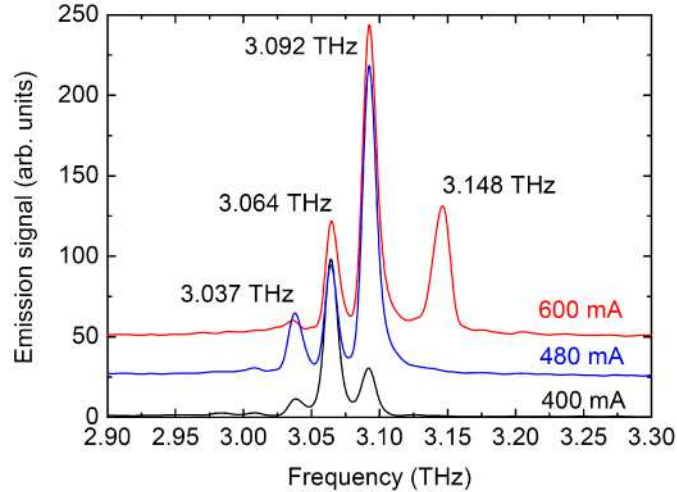
Fig. 5. Emission spectra of the QCL measured with a Fourier transform spectrometer for 400, 480, and 600 mA at 39, 44, and 52 K, respectively. The spectral resolution is approximately 10 GHz. The spectra are shifted for clarity. Several longitudinal modes of the Fabry-Pérot laser cavity separated by 28 GHz appear. Only the four strongest modes are labeled with their frequency. The frequency coverage is approximately 250 GHz.

The emission spectrum of the QCL was measured with a Fourier transform spectrometer and a liquid-helium-cooled Ge:Ga photoconductive detector. Three spectra measured for 400, 480, and 600 mA at 39, 44, and 52 K, respectively, are shown in Fig. 5. The spectral resolution is approximately 10 GHz. Several emission peaks are observed, which are separated by 28 GHz covering a range of approximately 250 GHz. These are the longitudinal modes of the Fabry-Pérot laser cavity. Their frequency separation is given by $\Delta v = c/(2n_{eff} L)$, with $c$ denoting the speed of light, $n_{eff}$ the effective refractive index of the active medium, and $L$ the length of the laser cavity. With $\Delta v = 28$ GHz and $L = 1.43$ mm, this yields $n_{eff} = 3.75$. Within the spectral resolution, none of the modes exhibits any frequency shift. The lack of any measureable frequency shift indicates a tunability of less than 10 GHz/200 mA = 50 MHz/mA. With increasing current, the output power increases, more modes appear, and the modes at higher frequencies become more intense relative to the lower frequency ones. This is probably caused by two optical transitions involved in the lasing process and a change in the relative population of the two emitting subbands [14].

## 4. Imaging

For imaging applications, transforming the output beam of the laser into a Gaussian-shaped beam with a small waist is a prime necessity. In order to achieve this condition, a lens made from polymethylpentene (PMP, trade mark TPX) with a focal length of 65 mm was positioned in such a way that the QCL was approximately in the focus of the lens. At the position of the minimum beam waist, which is 310 mm from the QCL, the beam profile was measured by scanning a sharp metal blade in steps of 0.1 mm across the beam. A Golay cell detector behind the blade registered the transmitted intensity. The result of this measurement is shown in Fig. 6. For a perfectly Gaussian-shaped beam, the intensity on the detector as a function of the blade position is given by the following relation

$$I(x) = I_0 \frac{1}{2} \left[ 1 + \mathrm{erf}\left( 2\sqrt{\ln 2} \, \frac{x - x_c}{d} \right) \right], \tag{1}$$

where $I_0$ denotes the total intensity of the beam, $x$ the position of the blade, and $x_c$ the position of the center of the distribution. The width $d$ of the distribution, which is defined as the distance between the positions of the blade where 11.9% and 88.1% of the full intensity are

transmitted, corresponds to the full width at half maximum (FWHM) of a Gaussian beam. The error function in Eq. (1) is obtained by integration of the Gaussian distribution. The measured distribution was fitted with Eq. (1), and the corresponding result is also shown in Fig. 6.
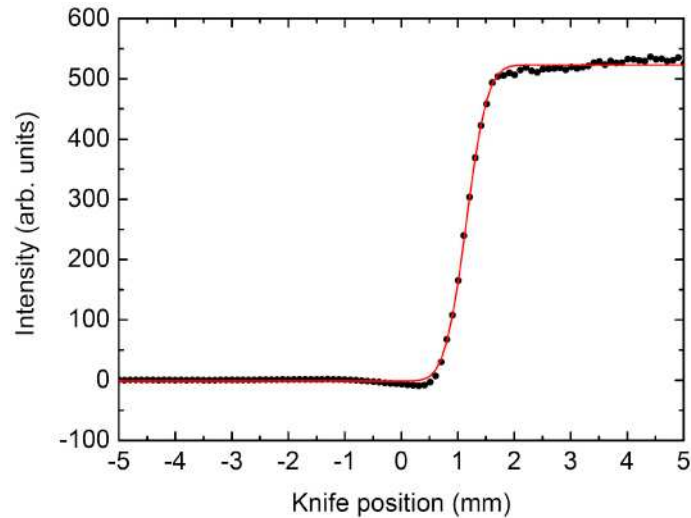


Fig. 6. Measurement of the beam profile at the position of the minimum waist by scanning a sharp metal blade in steps of 0.1 mm across the beam. The black squares are measured data points and the red curve is a fit to Eq. (1). The width is 700 µm.

There is a very good agreement between the measured and the fitted curve, which yields $d$ = $(0.70 \pm 0.01)$ mm. In addition, the beam profile at the position of the minimum beam waist was also measured by scanning a Golay cell detector with an aperture of 0.4 mm diameter in a plane orthogonal to the emission direction of the QCL. The result is shown in Fig. 4(b). The profile is slightly elongated, which is probably a remnant caused by the rectangular front facet of the laser. A Gaussian profile was fitted to the measured profile. The difference of the measured and the fitted Gaussian profile is shown in Fig. 4(c) in percent of the peak intensity. The deviation varies between +4.5% and −8.8%. The difference shows a ring-like pattern, which is most likely due to remaining interference and diffraction effects probably at the vacuum window or the TPX lens. The Rayleigh range of the optical system is approximately 10 mm as derived from the beam profile measurements. Despite these slight imperfections, the beam profile is sufficient for THz imaging applications with a spatial resolution below 1 mm.
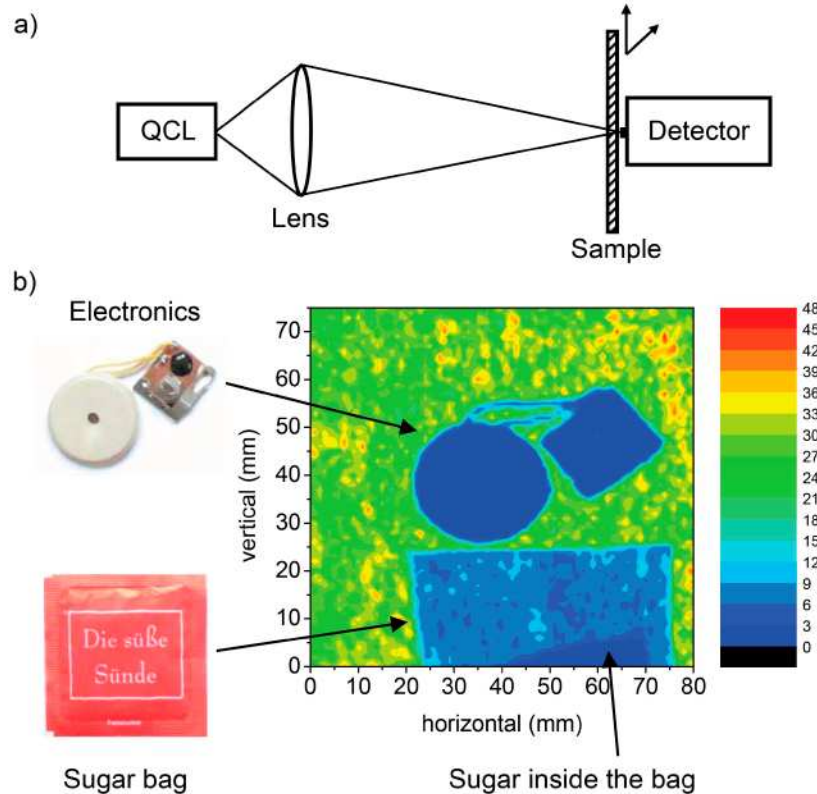
Fig. 7. a) Simplified scheme of the imaging setup: The sample is raster-scanned at the position of the minimum beam waist created by the TPX lens. b) THz image of a sugar bag and the electronic components of a music greeting card inside an envelope. The envelope was raster-scanned in steps of 1 mm through the position of the minimum waist. The legend shows the intensity of the transmitted signal (in arbitrary units).

To demonstrate the feasibility of the QCL source for imaging applications, we have taken a THz transmission image of a sugar bag and the electronic components of a music greeting card (Fig. 7). Both were enclosed in a standard envelope, which was raster-scanned in steps of 1 mm through the position of the minimum beam waist created by the TPX lens as described above. A Golay cell detector with a 1 mm aperture was placed directly behind the envelope. The output of the QCL was mechanically chopped at 12 Hz, and the signal was detected with a lock-in amplifier. The image has a dimension of $8 \times 7.5$ cm$^2$ and consists of 6000 pixels. Each pixel was taken with a time constant of 300 ms for the lock-in amplifier. Taking into account 600 ms for the movement of the raster-scanner from one pixel to the next one, the total time for acquiring the image was 1.5 hours. The electronic components are clearly visible, and the wires, which have a 1 mm diameter, are just resolved. The sugar bag is clearly visible as well as the fill level of the sugar inside the bag.

## 5. Toward high-resolution spectroscopy

As a first demonstration of the capability of the compact QCL source for spectroscopic applications, the absorption of $^{12}CH_3OH$ was measured with high spectral resolution around 3.1 THz. The experiment was performed by changing the current of the QCL and detecting the laser emission after transmission through an absorption cell. In this way, the laser frequency of each mode can be tuned over a spectral region of less than 10 GHz by changing the laser drive current across the whole range. The experimental setup is shown in Fig. 8.
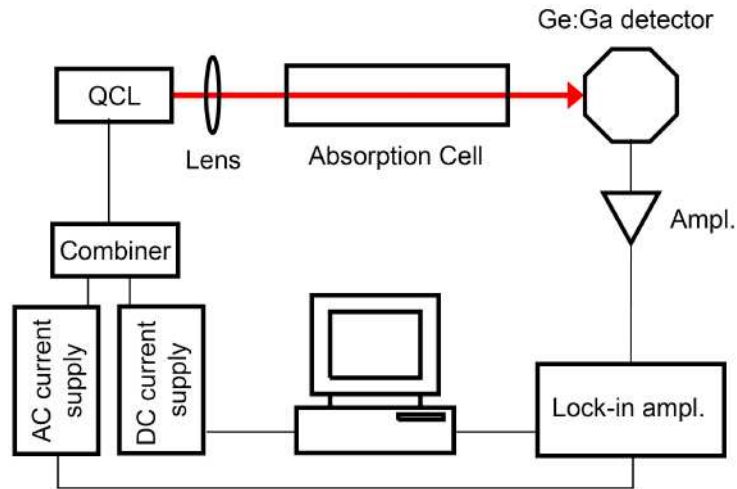
Fig. 8. Experimental set-up for gas-phase spectroscopy.

The diverging QCL beam was focused with the same TPX lens as for the imaging experiment through a 52-cm-long absorption cell onto a Ge:Ga detector, which was followed by a low-noise amplifier. The vacuum windows of the cell were tilted in order to avoid standing waves. The cell was filled with $^{12}CH_3OH$ at a pressure of 4.4 hPa measured with a capacitive manometer. The current of the QCL was modulated at a frequency of 10 kHz with a peak-to-peak amplitude of 1.6 mA by superposition of the modulation current from a frequency synthesizer with a DC current. The output signal from the low-noise amplifier was detected with a lock-in amplifier using the 10 kHz current modulation as a reference and an integration time of 1 ms. This results in a derivative-like absorption signal.
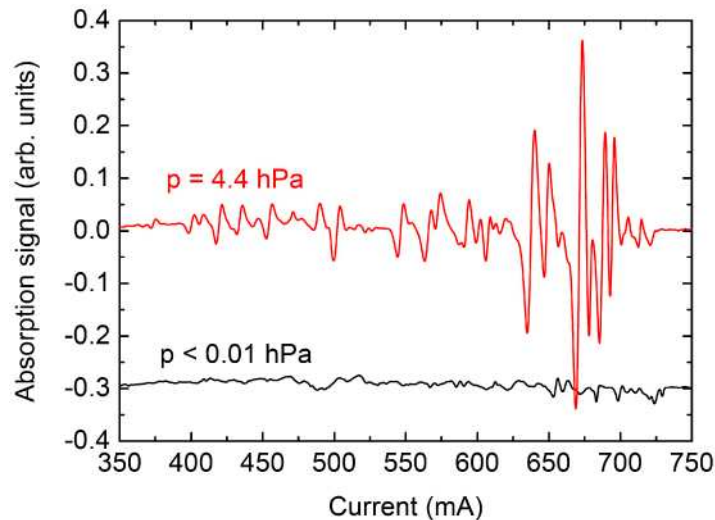


Fig. 9. Absorption signal of $^{12}CH_3OH$ as a function of laser current at 53 K for 4.4 hPa (red curve) and below 0.01 hPa (black curve). The black curve is shifted by −0.3 for clarity. Each scan took only 320 ms. The maximum signal-to-noise ratio is 1500.

As an example, the absorption signal is shown in Fig. 9 as a function of the laser current for pressures of 4.4 hPa and < 0.01 hPa. The recording time for the whole spectrum amounted to only 320 ms. At 4.4 hPa, absorption signals appear across the whole range of QCL drive current. The lock-in detection yielded a signal-to-noise ratio (SNR), which is as large as 1500 despite the short measurement time. A different detector, for example a Golay cell or a

pyroelectric detector, which have approximately a 100-1000 times higher noise-equivalent power, would either result in a correspondingly lower SNR or require longer integration times or higher laser powers. Using a detector with a sensitivity that is a hundred times smaller, a similar spectrum might be measured with a four times larger laser power and about six hundred times longer integration time, which corresponds to a total acquisition time of about 200 s.

The rather complicated absorption structure is due to the multimode operation of the laser, because each mode generates its own spectrum (Fig. 5). At this stage, it is rather difficult to identify certain transitions, because due to the large number of absorption lines of methanol a precise knowledge of the absolute frequency (to well below 1 GHz) and the tuning rate (to an accuracy of about 1 MHz/mA) are required. Therefore, normalization with respect to the laser power of the different modes has not been attempted. The FWHM of the absorption lines has been determined from the corresponding derivative-like signals. It is approximately 4 mA. Although the pressure broadening coefficients of these particular absorption lines have not been reported in the literature, it is reasonable to assume that they are about the same as for other methanol transitions [7]. Therefore, we can expect a FWHM of about 100 MHz at 4.4 hPa. This indicates a frequency tunability of around 25 MHz/mA in agreement with the upper limit established by the Fourier transform spectra (50 MHz/mA).

## 6. Summary and conclusion

In summary, we have realized a compact, cw THz source based on a QCL and a miniature cryocooler. Imaging and spectroscopy experiments show promising results. Further improvements are envisaged. The broad frequency coverage of almost 10% of the emission frequency [14] makes it attractive for implementation into an external cavity. This will allow for tuning of the emission frequency across a broad range as required for a spectrometer. Furthermore, the water-cooled Stirling cooler, which was used because it was readily available, will be replaced by an air-cooled instrument, which provides the same cooling capacity as the water-cooled one. Initial experiments with an air-cooled Stirling cooler show the same results as with the water-cooled one, both in terms of cooler performance (cooling capacity and vibrations) and in terms of laser performance (output power and beam profile). Along with frequency stabilization by for example locking to an external reference such as the emission from a multiplied microwave source [19, 20] or to a molecular absorption line [21], this source is an attractive option for a THz local oscillator. The results indicate that future developments of this source may result in many scientific or even commercial applications.